Design and manufacturing of bulk tungsten tiles for WEST outer limiter

M. Firdaouss, P. Chappuis, S. Gazzotti, M. Lipa, C. Portafaix, M. Diez

Version of Record: https://www.sciencedirect.com/science/article/pii/S0920379620305482
Manuscript_33b28d0bda65a6d4591d378f80dc537b

Design and Manufacturing of Bulk Tungsten Tiles for WEST Outer Limiter

M. Firdaouss[a]*, P. Chappuis[a], S. Gazzotti[a], M. Lipa[a], C. Portafaix[a], M.Diez[a]
[a]*CEA, IRFM, Cadarache, 13108 Saint-Paul-lez-Durance, France*

Limiter objects are facing high loads, even if they are not as close to the plasma as divertor for example. Loads come from plasma interaction during the standard situation (heat loads) and during abnormal situation like disruption (electromagnetic loads, runaway electrons). In WEST, the initial guess was to use CFC tiles with a tungsten coating for the outer bumper limiter. After two campaigns, it appears that the power and quantity of runaway beams had been underestimated, leading to early damages of the coating on significant surfaces. A second attempt for the tiles is to use bulk tungsten. This should ensure a high resistance the runaway beams. The design is validated for the given specifications. The tiles are manufactured in early 2019, and used during the WEST operations later this year. The first observations show a good resistance to the runaway beam, as expected.

Keywords: plasma facing components, bulk tungsten, limiter, design

1. Introduction

The main objective of the WEST project is to manufacture and test an ITER-like actively cooled tungsten divertor, and provide a full tungsten tokamak environment [1]. Besides the ITER-like actively cooled plasma facing units to be tested at WEST lower divertor, other WEST Plasma Facing Components (PFCs) were designed, manufactured and qualified [2-4]. The present paper focuses on the outer bumper limiter, a plasma-facing component aiming at protecting the RF antennae during the ramp-up and ramp-down normal phases, but also from transient energetic event like disruption and runaway beam. To handle those heat loads, the component was originally made of a thick CFC tile [5, 6], bolted onto a water-cooled heat sink made of CuCrZr by the mean of a spring system. In total, the outer limiter was equipped with 36 CFC tiles, 8 of them located on the top and bottom part that are longer than the others to protect the coolant tubes beneath. To enhance the heat transfer, a thin carbon foil is placed between the tile and the heat sink. The limiter is mounted on a movable arm, to cope with the needs of the RF antennae.

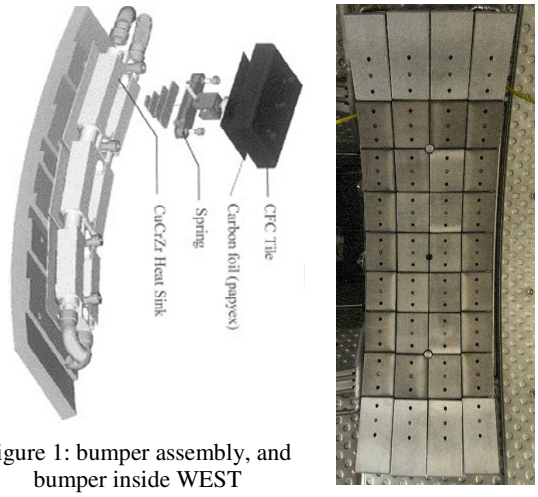

Figure 1: bumper assembly, and bumper inside WEST

This component has been successfully employed during the Tore-Supra CIEL operation. As the essential prerequisite of WEST is to operate in a metallic environment, development were supported by CEA in order to modify the plasma-facing material. A 100µm coating layer of tungsten (W) was then deposited onto the CFC substrate with a 100µm interlayer of molybdenum (Mo) by vacuum plasma spraying [4].

2. Lessons learned from WEST first campaigns

Among the various operations required during WEST shutdowns, PFC experts dedicate time to the in-situ inspection of PFC, in order to detect early failures. After the second WEST campaign (C2, 95.5MJ heating power during 1553s, 716 pulses), in early 2018, observations on the outer bumper have shown important delamination and melting of the coating on large areas of the bumper, especially near the mid-plan (fig. 2a and fig. 3). Therefore, tiles have been replaced with the few available spares, and for some of them moved from an exposed location to a less exposed one. After the following campaign C3 (5GJ heating power during 7302s, 1076 pulses) (fig. 2c), direct observations shown also delamination near the central ridge.

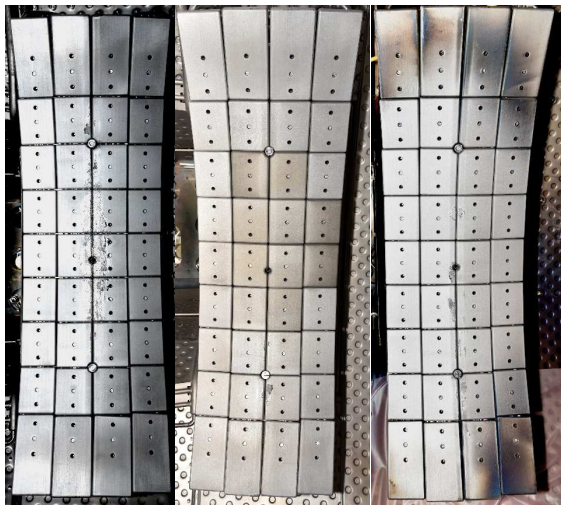

Figure 2: Bumper view from WEST- left to right: (a) after C2 (03/2018), (b) before C3 (05/2018), (c) after C3 (01/2019)

All these damages come from plasma disruption and subsequent runaway electrons, which were particularly

Author's email:mehdi.firdaouss@cea.fr

frequent during C2. However, even if disruption mitigation was improved during C3 (fig. 2), with lesser damages on coatings despite higher heating power and larger pulse number, it has been decided to look for a replacement solution, as power and duration were expected to increase for the following C4 campaign.

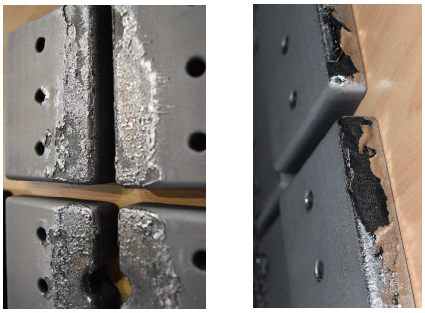

Figure 3: Close-up on delaminated / melted area on the central tiles surface (left) and on the edge of the lateral tiles (right) after C2

This article reports the adopted solution, which is to replace the W coated CFC tiles for bulk W tiles, with similar dimensions. The first part of the paper gives an overview of the main results during the design phase, giving details on the mechanical loads of the whole bumper assembly, then on the thermal analysis on an individual tile during plasma operations, and finally on a tile during a disruption, with the electro-magnetic loads. The second parts shows the manufactured tiles, and reports on the installation on WEST. The paper concludes on the behavior of the outer bumper during the C4a campaign (June-August 2019).

3. Load specifications and design

3.1 Mechanical analysis of the bumper assembly system

The first issue to be solved when changing CFC to W is simply due to the density of W material, which is ten times higher. On WEST, the risk is magnified by the fact that the 300kg mass of the whole assembly (130kg W + 170kg structure) is mounted on a steel tube, with a 800mm lever arm (fig. 4). To allow for radial displacement, the tube has a sliding contact. In addition to the mass, a 30kN.m torque is added to take into account the electro-magnetic forces.

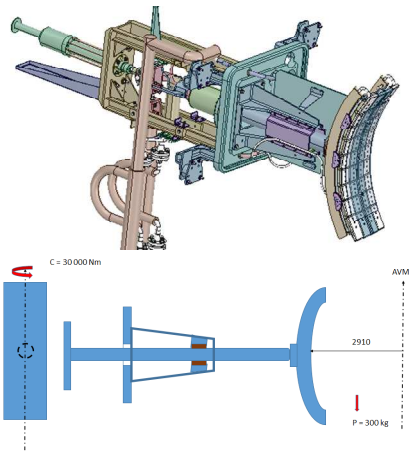

Figure 4: Bumper CAD model (left) and simplified model for simulation (left)

The structure is modeled using Ansys for two load cases: nominal temperature (70°C) with mass torque moment due to electromagnetic forces, and baking temperature (200°C) with mass only, as there is no plasma. Analysis of the results is done using the RCC-MR rules. The allowable stress (S_m) is defined as the minimum value of 2/3 of the yield stress and 1/3 of the ultimate stress. The primary membrane stress (P_m) is then compared to S_m, and the sum of the primary membrane stress and the primary bending stress (P_m+P_b) is compared to 1.5S_m. Results are indicated on table 1.

Table 1: P_m and P_m+P_b stresses for nominal and baking cases. RCC-MR criterion indicated in italic.

Case	P_m (MPa)	P_m + P_b (MPa)
Nominal	106 / *127*	127 / *191*
Baking	104 / *123*	124 / *185*

Conclusion is that the supporting system of the outer bumper is able to withstand both the weight of the new W bulk tiles (at 70°C and 200°C) and the electro-magnetic loads created during a disruption.

3.2 Thermo-mechanical analysis of an individual tile

3.2.1 Thermal analysis

The maximal thermal stress for the outer bumper is expected to be during the ramp-up phase. Indeed; at this stage, plasma may be in contact with the outer bumper, with a power up to 1MW, corresponding to 1MA plasma current, for a short time, typically lower than 1s. To assess the thermal effects, heat load simulation is carried out using PFCFlux [7]. Several scenarios are considered. Only the most conservative is reported here, with a decay length of 5mm. The heat flux resulting from this configuration is shown in fig. 5.

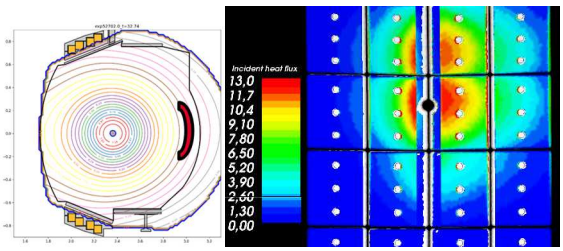

Figure 5: plasma equilibrium during ramp-up and resulting heat fluxes (MW/m²) on outer bumper

The heat flux may reach up to 13MW/m² on a small area for a duration estimated up to 1s. The thermo-mechanical simulation is done subsequently using Ansys. The model takes into account only the two central tiles with the highest heat fluxes.

The other boundary conditions for the simulation are the following: 1.5kW/m².°C for the heat transfer coefficient between the W tile and the cooling structure, 10kW/m².°C for the convection coefficient of coolant, and 100°C for the water temperature.

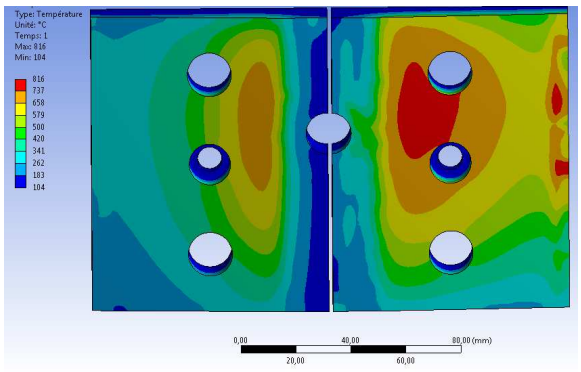

Figure 6: temperature after 1s heating on the two central tiles

After 1s heating, the maximal temperature is 816°C (fig. 6). This temperature stays lower than the tungsten recrystallization temperature, which is in the range of 1000°C. This ensures that the W material properties will not degrade over time.

3.2.2 Mechanical analysis

For the mechanical analysis, the tiles are attached to the spring support with a M8 stainless steel bolt, loaded with a 4000N pretension force. The contact between the tiles and the support is sliding with friction (0.3 friction coefficient). The resulting Von-Mises stress is shown on fig. 7.

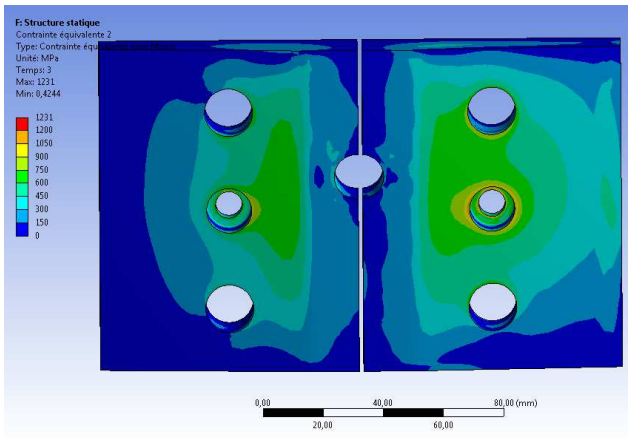

Figure 7: Von-Mises stress due to thermal dilatation on the two central tiles

As the stress comes from thermal solicitation, the criterion to take into account is the ultimate stress for the considered material. For tungsten, it is in the range of 1.0GPa. Some areas, localized near the edges of the fixation holes, are subject to stress close to this limit, or even slightly higher. This shows that the margins for this analysis case are very small, or even null.

This could be an issue, but the combination of thermal load level (1MA plasma current) and duration (1s), with plasma leaning on the outer bumper, is not the most common configuration in WEST. In addition, the 5mm decay length accounted in PFCFlux calculation is probably too conservative. This means that the margins will come from the experimental conditions. In addition, if the 1MA / 1s conditions are strongly requested for dedicated scenario, then two central tiles at the mid-plane should be carefully observed after operation, looking for traces of mechanical failure such as cracks on surface.

3.3 Mechanical analysis of an individual tile during disruptions

The last type of loading to be analyzed is the load during a disruption. Indeed, when the plasma collapses, the poloidal magnetic field changes very quickly. This field variation creates an electric current in the conductive material, in an orthogonal plan. Due to the presence at the same time of the toroidal magnetic field, Lorentz forces appear. The resulting load is a moment, which in return exerts a tensile force on the fixation bolt (fig. 8).

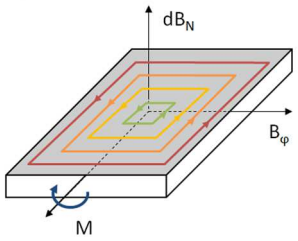

Figure 8: Electric current and resulting moment

After integration of the contribution of each current line, the total moment that is exerted on a rectangular object is:

$$M = \frac{a^3 b^3}{12(a^2+b^2)} \frac{e}{\rho} \frac{dB_n}{dt} B_\varphi$$

a and b are the surface dimensions, while e is the thickness. ρ is the electrical resistivity. B_n is the magnetic field normal to the surface, and B_φ the toroidal magnetic field.

3.3.1 Moments and forces without castellations

Two types of tiles are to be considered: standard and long. Both types have the same width (86mm) and thickness (20mm on average). Length are 107mm and 170mm respectively. The electrical resistivity is 8.5µW.cm at 160°C, which corresponds to an average temperature of the tile. Variation of the radial field is estimated to be 50T/s, while the nominal toroidal field is 3.3T.

Applying the previous formula, the moments are estimated to be 134N.m and 279N.m respectively for standard and long tiles. As the only fixation of the tile is the central bolt, a tensile force corresponding to the moment divided by the half-width (43mm) is exerted on the bolt. This means that the bolt supports a force of 3.1kN for the standard tile and 6.5kN for the long tile.

The mechanical limit on the fixation system does not come from the fixation itself, but from the spring system between the tile and the support. The primary role of the spring is to handle the deformation due to the thermal gradient. This spring can deform without plastic deformation up to 1.5kN. It breaks for a force higher than 1.8kN.

Obviously, the important stresses calculated above, coming from a disruption, may break the spring system. This would lead to a definitive failure of the fixation system.

3.3.2 Moments and forces with castellations

To overcome this important issue, loads during the disruption have to be reduced to an acceptable level. To ensure that, the common technique is to cut the electrical path, by adding castellations. For the current tiles, two vertical castellations are considered. The remaining tungsten thickness is 7mm (fig. 9).

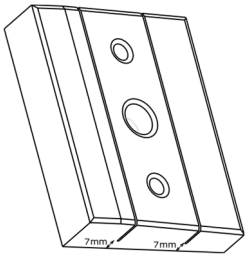

Figure 9: Schematic view of the new standard tile with two vertical castellations developed for WEST

A tile can then be considered as constituted by four independent blocks. The moment formula is applied on each of them, and the resulting moment is the sum of all the moments. With this method, the moment becomes 62N.m on the standard tiles and 121N.m for the long tiles. The force that applies on the bolt is finally 1.4kN and 2.8kN.

This result is acceptable for the standard tiles. However, there is still a risk that the spring system may fail during a disruption for the long tiles. To solve this limit, the spring system is replaced by a rigid one, similar in shape and fixation, but made of plain steel. This system is largely able to handle a force of 2.8kN.

4. Manufacturing and assembly in WEST

Due to the presence of a gas injection tube and two Langmuir probes, eight variants of the tiles are designed in total for the 36 tiles. The shape of the tiles surrounding the top and bottom Langmuir probes is specially designed to protect them from the runaway beam. The gap between the adjacent tiles are not aligned with the magnetic field lines (fig. 10).

It is also noticeable that the central bolt is made of Titanium/Molybdenum/Zirconium (TZM). This is a legacy from Tore Supra long duration operation. Indeed, for these operations, it was assumed that the temperature of these bolts might increase to several hundred of degrees. This temperature range is not compatible with standard steel bolts. TZM has been chosen among several materials as a compromise between mechanical performance and thermal endurance.

Requirements on tungsten material are similar to ITER ones [8], in particular grain size finer than 3 (ASTM grain size i.e. 127µm), hardness over 410 HV30 and purity higher than 99.94%.

The tiles are delivered to CEA in April 2019. A cautious inspection of the tiles is done, in order to detect initial cracks, scratches and defects. None of the manufactured tiles shows any of these defaults (fig. 10).

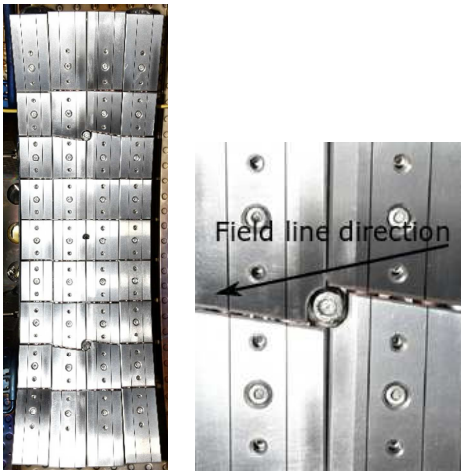

Figure 10: View of the outer bumper equipped with bulk W tiles before C4 (04/2019) (left) and close-up on Langmuir probe (right)

5. Conclusion

The first WEST campaign using this newly design limiter have started in June 2019, and should last until the end of the same year.

Using the Articulated Inspection Arm [9], a robot able to enter inside WEST without losing vacuum and conditioning, no surface defects have been observed after C4a (10GJ heating power during 9968s, 1157 pulses), although disruptions accompanied by runaway beam have still occurred. This demonstrates the superiority of the bulk W material over the W coatings regarding those very brief and intense events.

With the good results of the described change, from W coating to W bulk materials for the outer bumper, it is now expected to revise the six inner bumpers with similar modification. These bumpers are located on the high field side, and are very similar to the outer bumper in terms of requirements, the main difference being that the inner bumpers are not movable. This change will be included of the second part of WEST upgrade (WEST Phase II), which should be completed in May 2020. Phase II particularly focuses on the assembly, mounting and operation of a 360° bottom divertor made of W monoblock (ITER-like).

References

1 J. Bucalossi et al., 10.1016/j.fusengdes.2014.01.062, Fusion Eng. Des.89 (2014) 907

2 T. Batal et al., 10.1016/j.fusengdes.2015.01.053 Fusion Eng. Des. 98-99 (2015) 1221

3 M. Richou et al., 10.1016/j.fusengdes.2014.12.017 Fusion Eng. Des. 98-99 (2015) 1394

4 M. Firdaouss et al., 10.1016/j.fusengdes.2017.02.087, Fusion Eng. Des. 124 (2017) 207

5 P. Garin, 10.1016/S0920-3796(00)00346-X, Fusion Eng. Des. 49–50 (2000) 89

6 M. Lipa et al., 10.1016/S0920-3796(03)00217-5, Fusion Eng. Des. 66–68 (2003) 365
7 M. Firdaouss et al., 10.1016/j.fusengdes.2014.12.024, Fusion Eng. Des. 98–99 (2015) 1294
8 Barabash V. and Hirai T., Tungsten Plate Specification for Divertor PFC, 2EDZJ4 v2.2, nov 2017
9 V. Bruno et al., 10.1016/j.fusengdes.2018.11.050, Fusion Eng. Des. 146 (2019) 115